Supporting Information (SI):

High-density low-coordination Ni single atoms anchored on Ni-embedded nanoporous carbon nanotubes for boosted alkaline hydrogen evolution

Liangliang Feng[a,b*], Changle Fu[a], Dongming Li[a], Xuan Ai[c*], Hongyan Yin[a], Yuhang Li[a], Xiaoyi Li[a], Liyun Cao[a], Jianfeng Huang[a*]

[a] *School of Materials Science & Engineering, Shaanxi Key Laboratory of Green Preparation and Functionalization for Inorganic Materials, Shaanxi University of Science & Technology, Xi'an Shaanxi, 710021, P.R. China*

[b] *Key Laboratory of Advanced Energy Materials Chemistry (Ministry of Education), Nankai University, Tianjin 300071, China*

[c] *School of Materials Science and Engineering, Key Laboratory of Macromolecular Science of Shaanxi Province, Key Laboratory of Applied Surface and Colloid Chemistry (Ministry of Education), Shaanxi Key Laboratory for Advanced Energy Devices, Shaanxi Engineering Lab for Advanced Energy Technology, Shaanxi Normal University, Xi'an 710062, PR China*

[*] Corresponding authors.

E-mail addresses: fengll@sust.edu.cn (L. Feng); aixuan1995@163.com (X. Ai); huangjf@sust.edu.cn (J. Huang)

Number of pages: 20

Number of figures: 24

Number of tables: 3

Containing 20 pages, 24 Figures and 3 Tables

Additional images and data:

Figure S1. XRD pattern of the NiAl-LDH precursor.

Figure S2. XRD pattern obtained from Ni-N-C/Ni/AlN@CNT after alkali treatment and high temperature calcination in Ar atmosphere.

Figure S3. XRD pattern of the $Ni(OH)_2$ precursor.

Figure S4. N_2 adsorption-desorption isotherms of the Ni-N-C/Ni/AlN@CNT and Ni-N-C/Ni@CNT.

Figure S5. SEM image of the Ni-N-C/Ni/AlN@CNT.

Figure S6. SEM images with different magnifications of the (a-c) Ni-N-C/Ni@CNT-H and (d-f) Ni-N-C/Ni@CNT-L.

Figure S7. (a) TEM image and (b) high-resolution TEM image of Ni-N-C/Ni/AlN@CNT; (c) STEM image and the corresponding EDX mapping images of C, N, Ni and Al elements.

Figure S8. The XPS survey spectra and the corresponding elemental contents of the Ni-N-C/Ni@CNT-H and Ni-N-C/Ni@CNT-L.

Figure S9. (a) C 1s high-resolution XPS spectra of the Ni-N-C/Ni@CNT-H and Ni-N-C/Ni@CNT-L; (b) Al 2p high-resolution XPS spectrum of the Ni-N-C/Ni@CNT-H.

Figure S10. The preparation procedure of the catalyst slurry.

Figure S11. XRD patterns of (a) NiAl-LDH and (b) Ni-N-C/Ni/AlN@CNT prepared at different ingredient ratios.

Figure S12. SEM images of the Ni-N-C/Ni/AlN@CNT fabricated under Ni:Al conditions at 1.8:1 and 3:1.

Figure S13. LSV curves of the Ni-N-C/Ni/AlN@CNT prepared at different ingredient ratios.

Figure S14. (a) XRD patterns and (b) Raman spectra of Ni-N-C/Ni/AlN@CNT produced at different calcination temperatures.

Figure S15. SEM images of Ni-N-C/Ni/AlN@CNT produced at different calcination temperatures. (a) 700 ℃; (b) 900 ℃ and (c) 1000 ℃.

Figure S16. LSV curves of Ni-N-C/Ni/AlN@CNT produced at different calcination temperatures.

Figure S17. (a) XRD pattern of the AlN and (b) LSV curves of the AlN and Ni-N-C/Ni@CNT-H.

Figure S18. LSV curves of the Ni-N-C/Ni@CNT-H, Ni-N-C/Ni@CNT and Ni-N-C/Ni/AlN@CNT.

Figure S19. Cyclic voltammetry curves of the samples with different scanning rates (10, 20, 40, 60, 80, 100 mV s^{-1}) for HER in 1 M KOH electrolyte. (a) Ni-N-C/Ni@CNT-H and (b) Ni-N-C/Ni@CNT-L.

Figure S20. Normalized LSV curves by ECSA of Ni-N-C/Ni@CNT-H and Ni-N-C/Ni@CNT-L.

Figure S21. The polarization curves of Ni-N-C/Ni@CNT-H before and after 5000 CV cycles.

Figure S22. (a) TEM image and (b-d) he corresponding mapping images of C, N and Ni elements of the Ni-N-C/Ni@CNT-H.

Figure S23. XPS spectra of the Ni-N-C/Ni@CNT-H after HER electrochemical test in 1 M KOH: (a) Wide spectrum; (b) C 1s; (c) Ni 2p; (d) N 1s.

Figure S24. Stability test at current density of 240 mA cm^{-2} of Ni-N-C/Ni@CNT-H in alkaline condition.

Table S1. (a) The details for calculated fractions of each nitrogen species in the N 1s XPS spectrum. (b) The details of the proportion of each N species in the whole sample were derived from the calculations.

Table S2. EXAFS fitting results of Ni-N-C/Ni@CNT-H and Ni foil.

Table S3. Comparison of HER performance between the results from the present research with recently-reported single-atomic electrocatalysts in 1 M KOH.

Theoretical calculation:

The HER process is divide into the two fundamental reactions as following：

（1） $H+ e^- + * = {}^*H$

（2） ${}^*H = * + 1/2\ H_2$

${}^*H$ presents the H moiety on the adsorption site. Where which the energy of H^+/e^- is approximately equal to the energy of 1/2 H_2.[1]

The change in Gibbs free energy (ΔG) of each adsorbed intermediate was calculated based on the computational hydrogen electrode method developed by Nørskov et al. At standard condition (T = 298.15 K, pH = 0, and U = 0 V (vs. SHE)), the free energy G is defined as the following equation:

$$\Delta G = \Delta E + \Delta E_{ZPE} - T\Delta S$$

Where ΔE is the energy change obtained from DFT calculation, ΔE_{ZPE} is the difference between the adsorbed state and gas, which is calculated by summing vibrational frequency for all model based on the equation: $E_{ZPE} = 1/2 \sum h\nu_i$ (T is the temperature (298.15 K) in the above reaction system, and ΔS represents the difference on the entropies between the adsorbed state and gas phase. The entropies of free molecules were obtained from NIST database. And the free energy of the adsorbed state *H can be taken as: $\Delta G_{*H}=\Delta E_{*H}+0.24$.[2]

The d-band center proposed by Nørskov and co-workers is a semi-quantitative descriptor to describe the trend of reactivity of transition metals.[3] A transition metal with a low ε_d value relative to the Fermi level, shows a weak adsorption for a given adsorbate. And the *d*-band center (ε_d) is calculated as following：

$$\varepsilon_d = \frac{\int_{-\infty}^{+\infty} x\rho(x)dx}{\int_{-\infty}^{+\infty} \rho(x)dx}$$

Where ρ(x) is the projector density of states (PDOS) with respect to Ni atom on Ni cluster, Ni (111), Ni-N_4, and Ni-N_2 catalysts. Among them, we calculated the d-band center of active Ni atom in Ni-N_4 and Ni-N_2 and the average d-band center of Ni atoms in Ni cluster and Ni (111). The energy range is from -10 to 10 eV.

Electrochemical active surface area (ECSA) calculation:

The ECSA of the electrode is estimated from the double-layer capacitance (C_{dl}) of the catalyst according to the following equation:[4,5]

$$ECSA = C_{dl} / C_s$$

Where, C_s is the specific capacitance of a flat standard electrode. In our estimates of ECSA, we take the general value of 40 μF cm^{-2} for C_s.

The LSVs normalized by ECSA of HER under alkaline electrolyte solution is derived from the equation:[6]

$$j_{ECSA} = j/ECSA$$

Where j represents the measured current density.

Turnover frequency (TOF) calculation:

In order to estimate the intrinsic activity of Ni-N-C/Ni@CNT-H, the turnover frequency (TOF) value was calculated from the following equation:[7-10]

$$\text{TOF } (s^{-1}) = \frac{j/nF}{m_{cat} \times \omega / M_{Ni}}$$

Where j is the HER partial current density (mA cm^{-2}), n is the number of electrons transferred for H_2 formation, F is the Faraday's constant (96,485 C mol^{-1}), m_{cat} is the catalyst loading on the electrode (0.94 mg cm^{-2}), ω is the Ni content of the

catalyst obtained by inductively coupled plasma-atomic emission spectroscopy (22.1%), M_{Ni} is the atomic mass of Ni (58 g mol^{-1}).

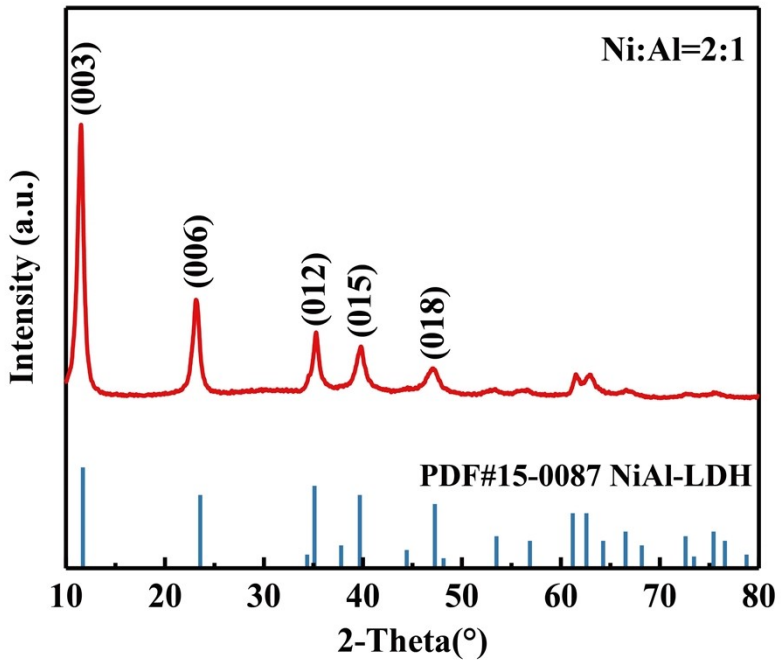

Figure S1. XRD pattern of the NiAl-LDH precursor.

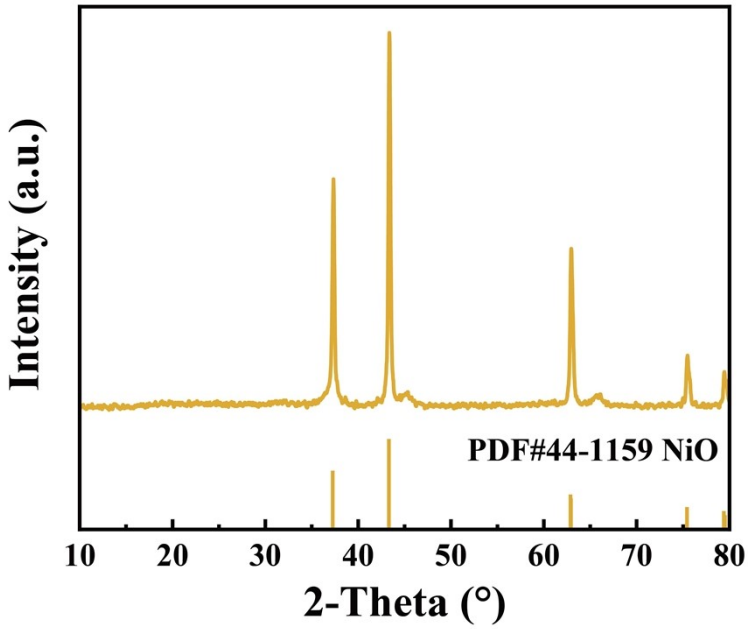

Figure S2. XRD pattern obtained from Ni-N-C/Ni/AlN@CNT after alkali treatment and high temperature calcination in Ar atmosphere.

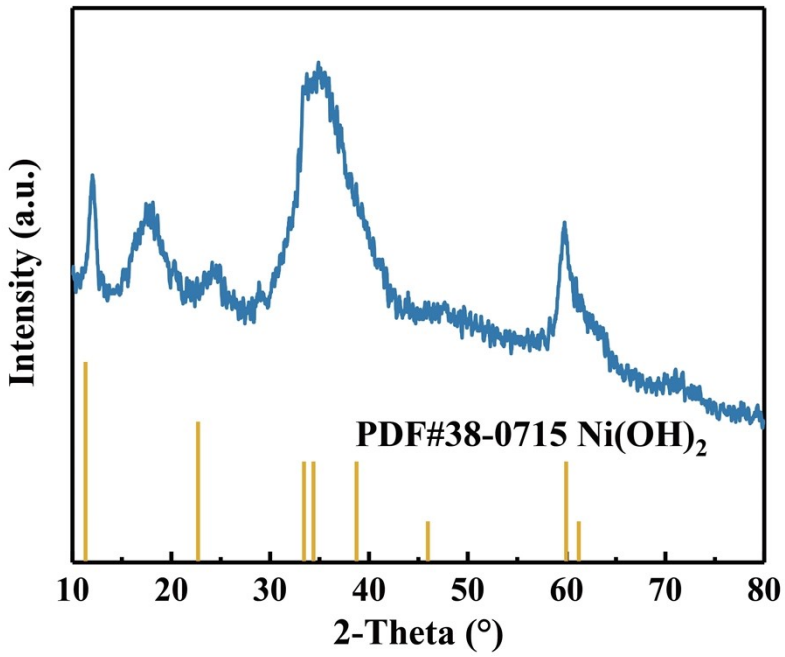

Figure S3. XRD pattern of the $Ni(OH)_2$ precursor.

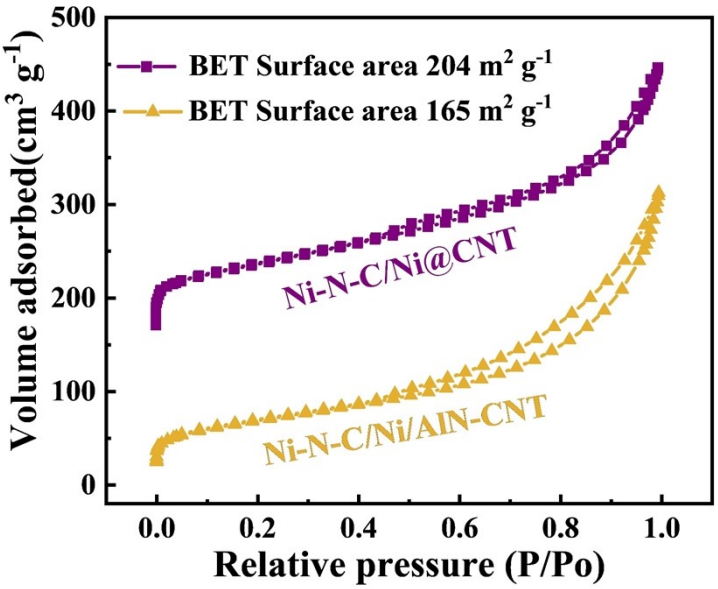

Figure S4. N_2 adsorption-desorption isotherms of the Ni-N-C/Ni/AlN@CNT and Ni-N-C/Ni@CNT.

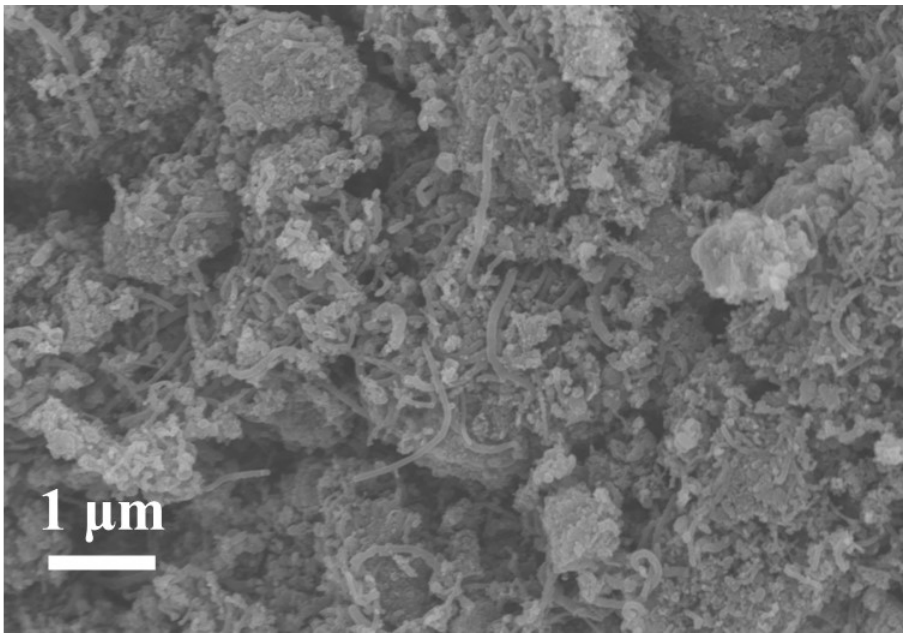

Figure S5. SEM image of the Ni-N-C/Ni/AlN@CNT.

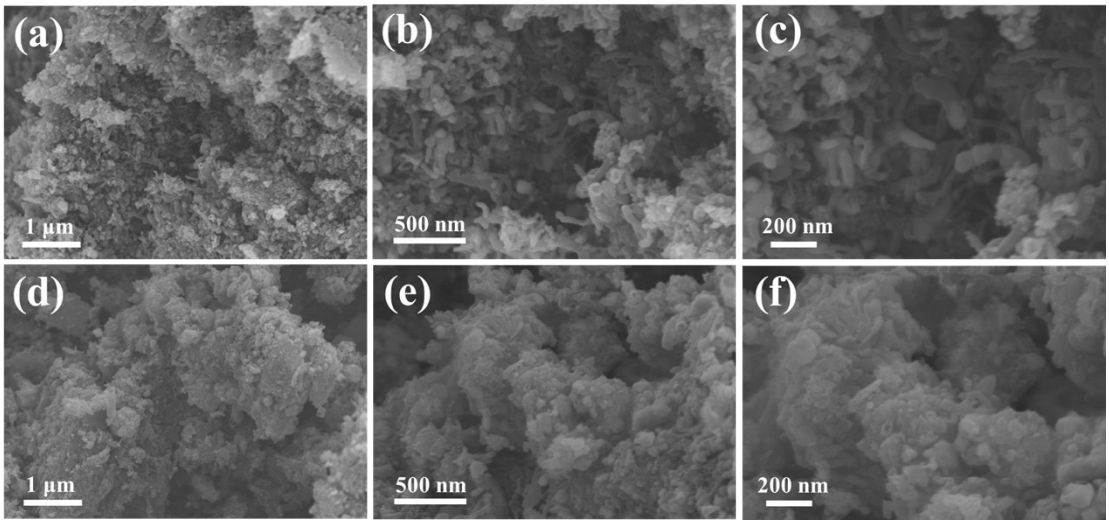

Figure S6. SEM images with different magnifications of the (a-c) Ni-N-C/Ni@CNT-H and (d-f) Ni-N-C/Ni@CNT-L.

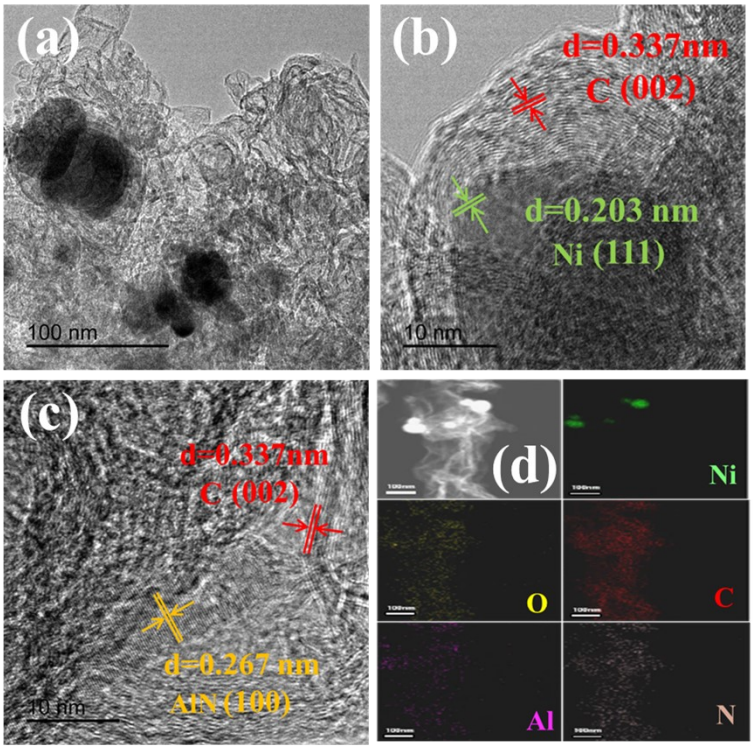

Figure S7. (a) TEM image and (b) high-resolution TEM image of Ni-N-C/Ni/AlN@CNT; (c) STEM image and the corresponding EDX mapping images of C, N, Ni and Al elements.

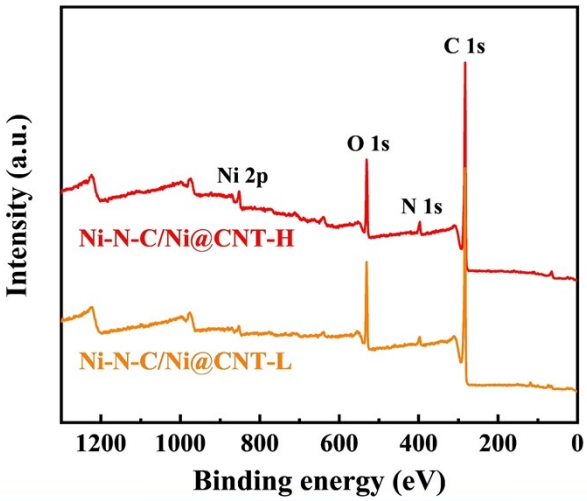

	C 1s	N 1s	Ni 2p	O 1s
Ni-N-C/Ni@CNT-H	74.22%	3.15%	12.66%	9.97%
Ni-N-C/Ni@CNT-L	79.48%	1.90%	7.54%	11.08%

Figure S8. The XPS survey spectra and the corresponding elemental contents of the Ni-N-C/Ni@CNT-H and Ni-N-C/Ni@CNT-L.

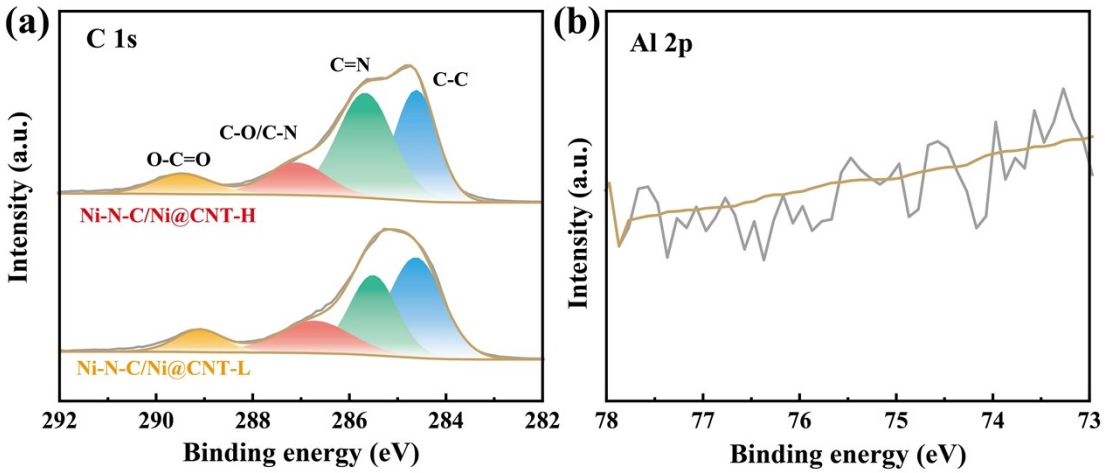

Figure S9. (a) C 1s high-resolution XPS spectra of the Ni-N-C/Ni@CNT-H and Ni-N-C/Ni@CNT-L; (b) Al 2p high-resolution XPS spectrum of the Ni-N-C/Ni@CNT-H.

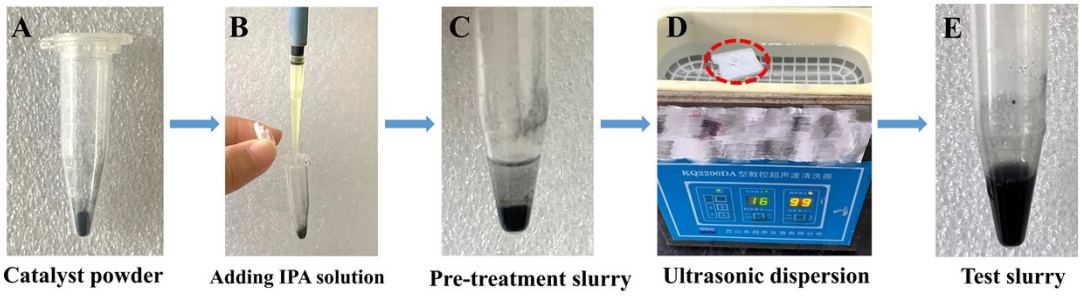

(A) 5 mg of catalyst powder was put into a 1.5 mL of centrifuge tube

(B) Adding 150 μL of isopropyl alcohol (IPA) solution into the centrifuge tube

(C) The stratified catalyst slurry was obtained before the ultrasonic treatment

(D) The above slurry was treated ultrasonically for 30 min

(E) Uniformly dispersed catalyst slurry was gotten for electrocatalytic HER

Figure S10. The preparation procedure of the catalyst slurry.

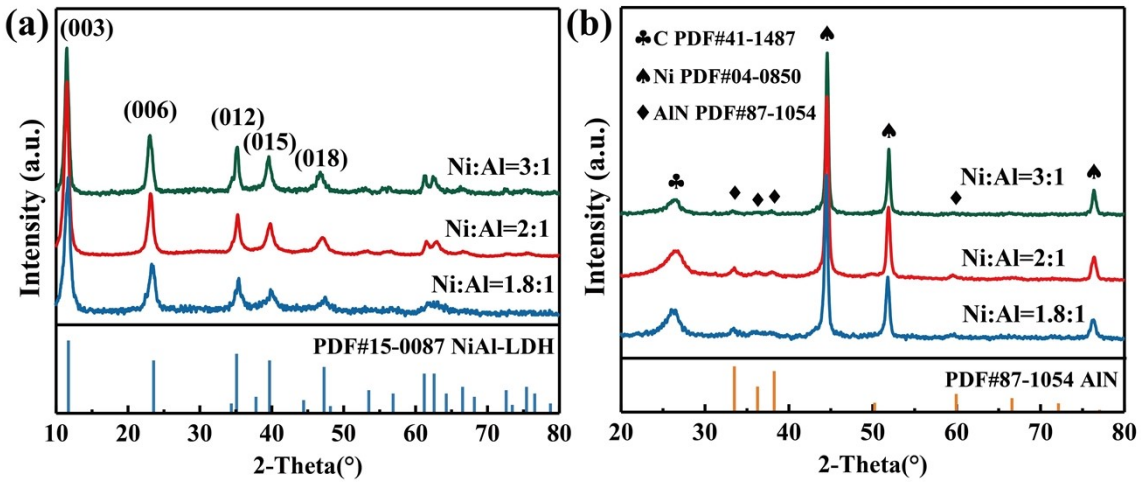

Figure S11. XRD patterns of (a) NiAl-LDH and (b) Ni-N-C/Ni/AlN@CNT prepared at different ingredient ratios.

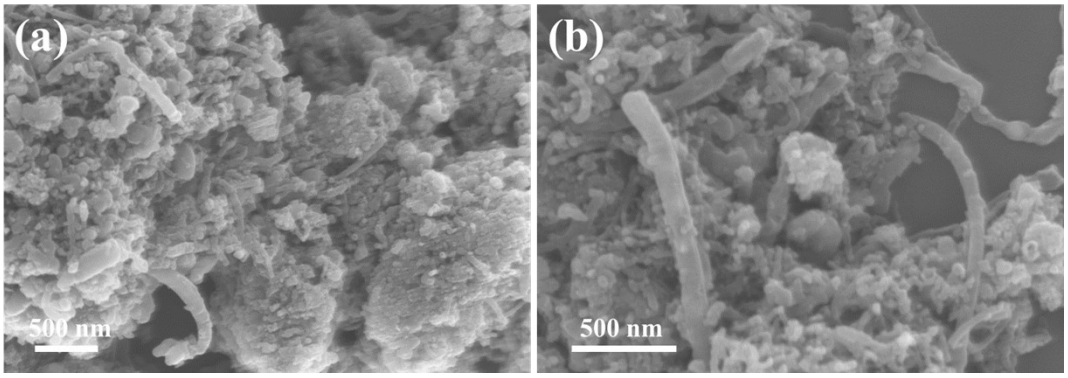

Figure S12. SEM images of the Ni-N-C/Ni/AlN@CNT fabricated under Ni:Al conditions at 1.8:1 and 3:1.

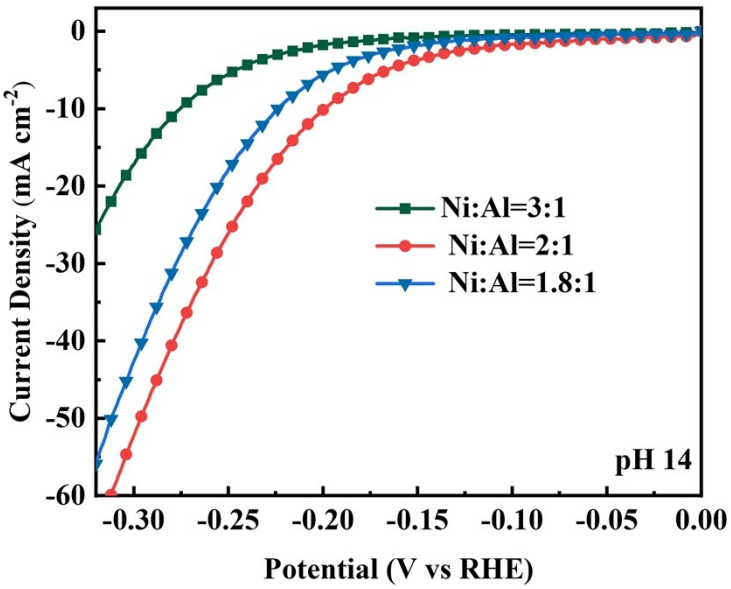

Figure S13. LSV curves of the Ni-N-C/Ni/AlN@CNT prepared at different ingredient ratios.

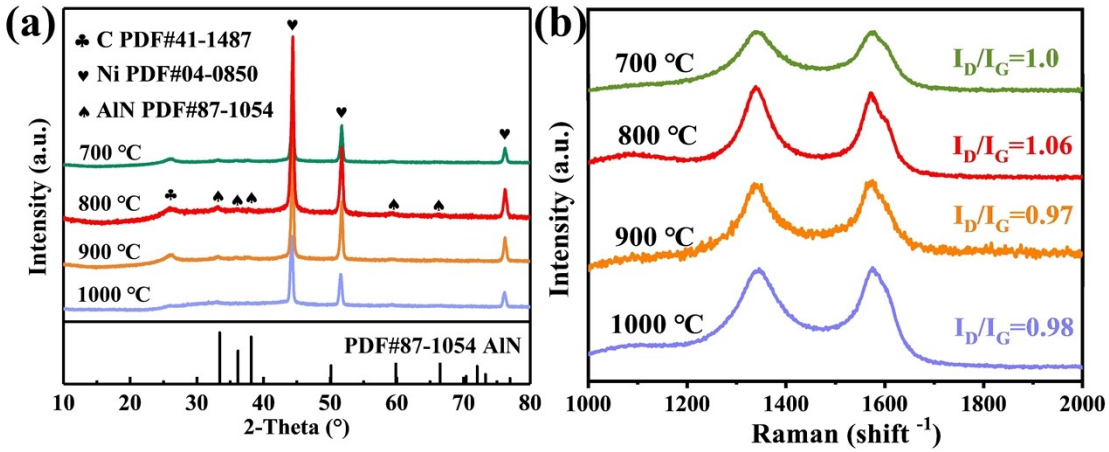

Figure S14. (a) XRD patterns and (b) Raman spectra of Ni-N-C/Ni/AlN@CNT produced at different calcination temperatures.

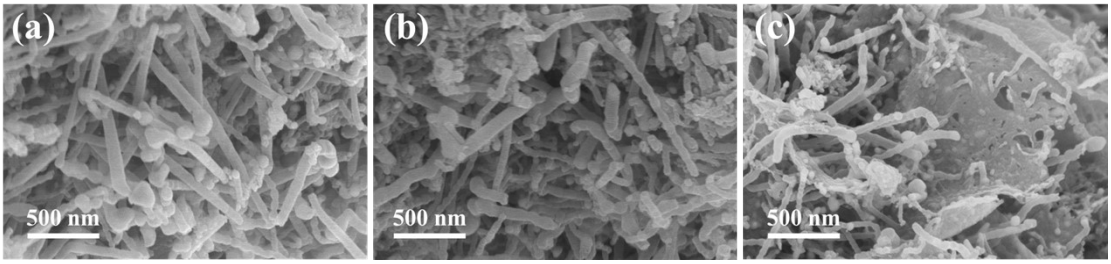

Figure S15. SEM images of Ni-N-C/Ni/AlN@CNT produced at different calcination temperatures. (a) 700 ℃; (b) 900 ℃ and (c) 1000 ℃.

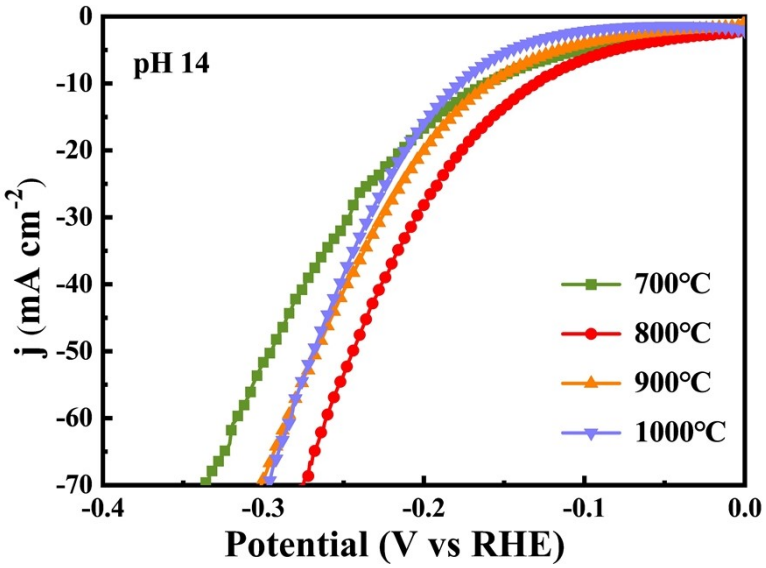

Figure S16. LSV curves of Ni-N-C/Ni/AlN@CNT produced at different calcination temperatures.

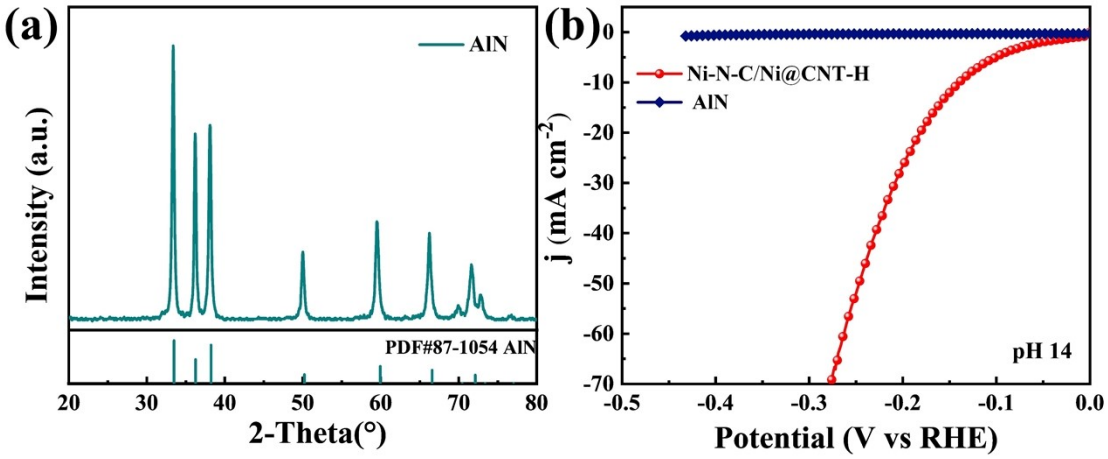

Figure S17. (a) XRD pattern of the AlN and (b) LSV curves of the AlN and Ni-N-C/Ni@CNT-H.

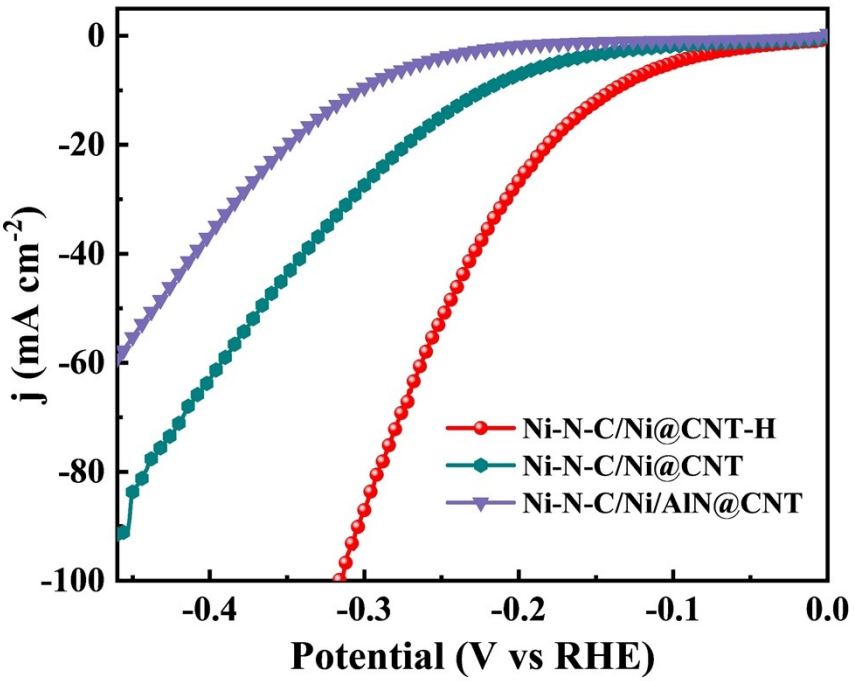

Figure S18. LSV curves of the Ni-N-C/Ni@CNT-H, Ni-N-C/Ni@CNT and Ni-N-C/Ni/AlN@CNT.

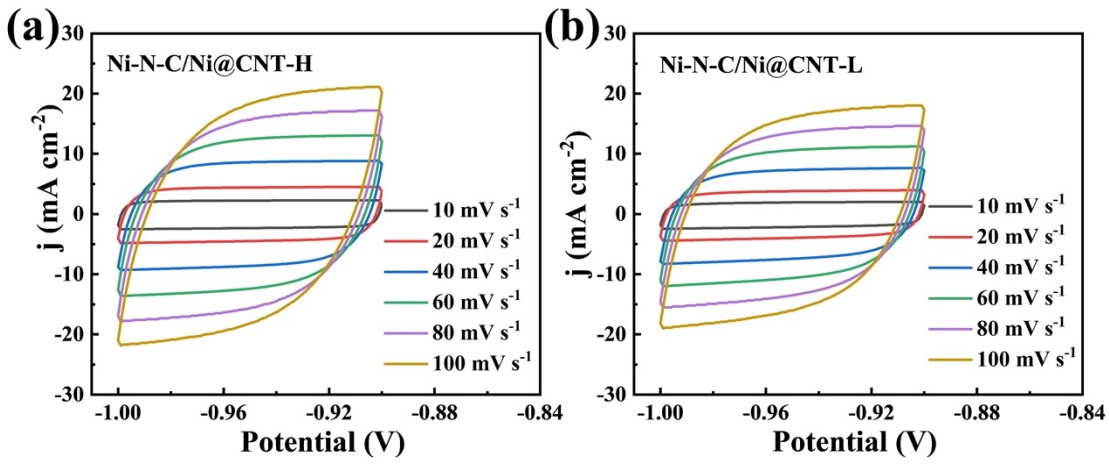

Figure S19. Cyclic voltammetry curves of the samples with different scanning rates (10, 20, 40, 60, 80, 100 mV s^{-1}) for HER in 1 M KOH electrolyte: (a) Ni-N-C/Ni@CNT-H and (b) Ni-N-C/Ni@CNT-L.

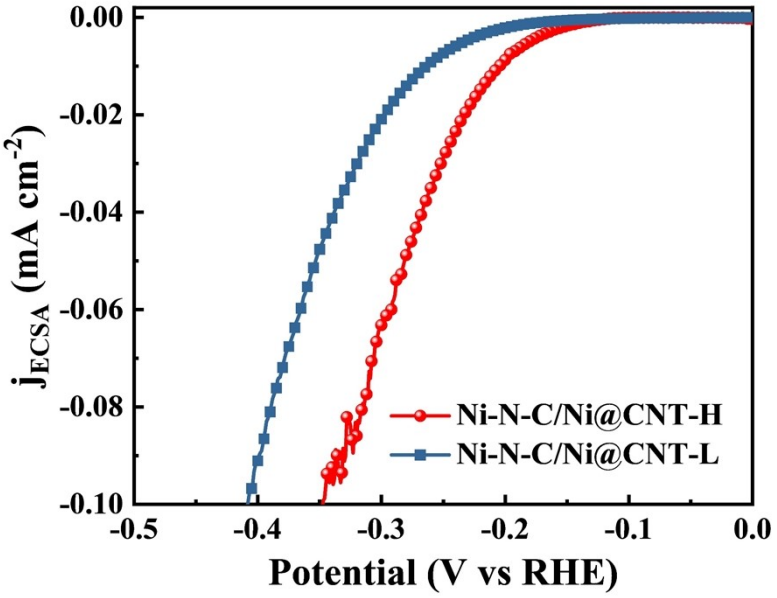

Figure S20. Normalized LSV curves by ECSA of Ni-N-C/Ni@CNT-H and Ni-N-C/Ni@CNT-L.

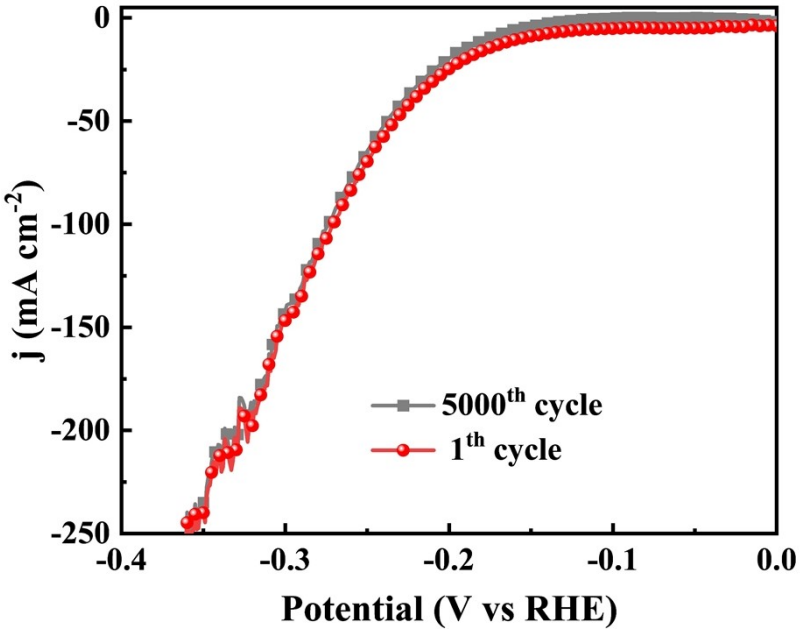

Figure S21. The polarization curves of Ni-N-C/Ni@CNT-H before and after 5000 CV cycles.

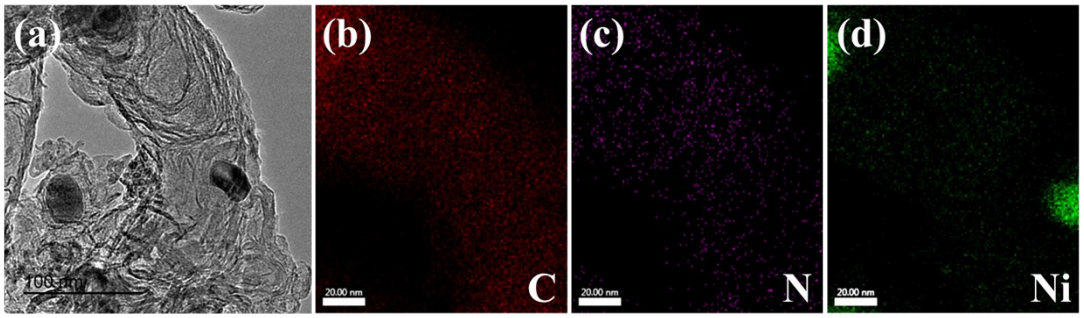

Figure S22. (a) TEM image and (b-d) he corresponding mapping images of C, N and Ni elements of the Ni-N-C/Ni@CNT-H.

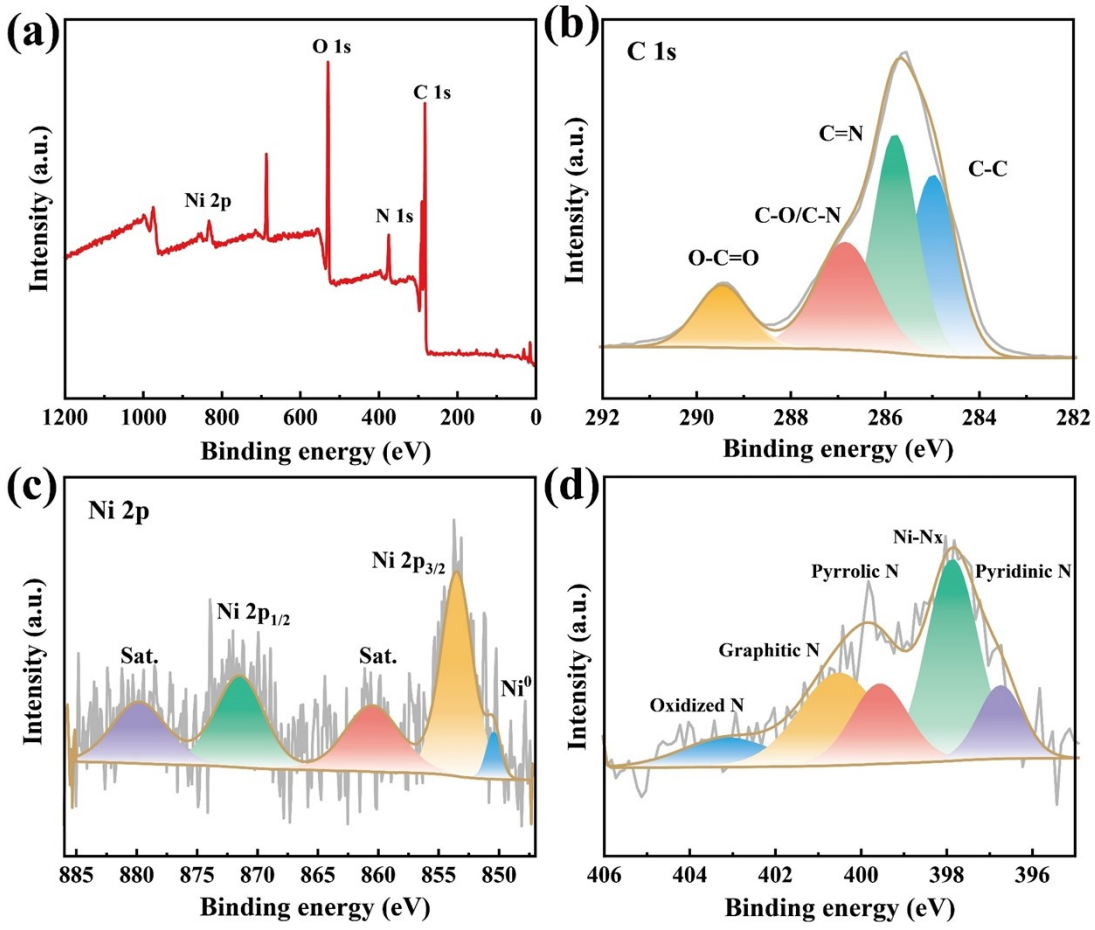

Figure S23. XPS spectra of the Ni-N-C/Ni@CNT-H after HER electrochemical test in 1 M KOH: (a) Wide spectrum; (b) C 1s; (c) Ni 2p; (d) N 1s.

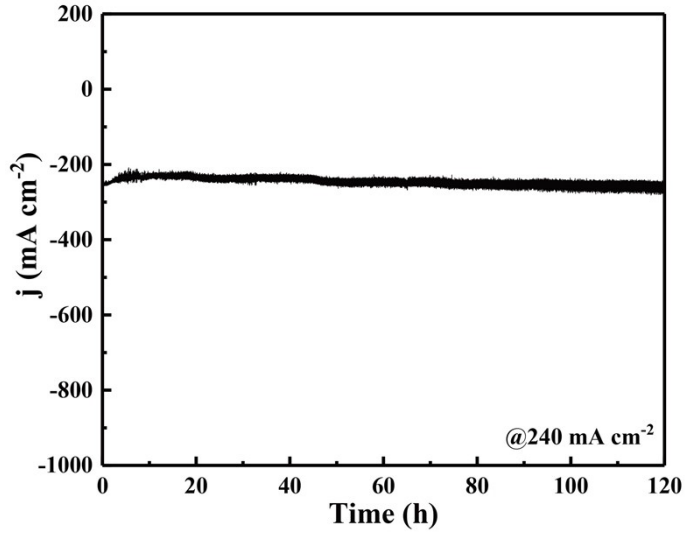

Figure S24. Stability test at current density of 240 mA cm^{-2} of Ni-N-C/Ni@CNT-H in alkaline condition.

Table S1. (a) The details for calculated fractions of each nitrogen species in the N 1s XPS spectrum.

Catalyst	Pyridinic N [%]	Ni-N_x [%]	Pyrrolic N [%]	Graphitic N [%]	Oxidized N [%]
Ni-N-C/Ni@CNT-H	9.08	36.11	17.51	28.55	8.75
Ni-N-C/Ni@CNT-L	11.64	29.47	19.39	28.18	11.32

Table S1. (b) The details of the proportion of each N species in the whole sample were derived from the calculations.

Catalyst	Pyridinic N [%]	Ni-N_x [%]	Pyrrolic N [%]	Graphitic N [%]	Oxidized N [%]
Ni-N-C/Ni@CNT-H	0.286	1.137	0.552	0.899	0.276
Ni-N-C/Ni@CNT-L	0.221	0.560	0.368	0.535	0.216

Table S2. EXAFS fitting results of Ni-N-C/Ni@CNT-H and Ni foil.

Sample	shell	N [a]	R (Å) [b]	σ^2 ($Å^2 \cdot 10^{-3}$) [c]	ΔE0 (eV) [d]
Ni foil	Ni-Ni	12	2.473±0.003	5.98±0.4	6.563±0.540
Ni-N-C/Ni@CNT-H	Ni-N	2.1±0.56	1.902±0.075	5.07±7.42	-5.979±3.34

	Ni-Ni	6.72±1.22	2.472±0.013	5.75±1.67	-6.892±2.49

[a] N: coordination numbers; [b] R: bond distance; [c] σ^2: Debye-Waller factors;

[d] ΔE_0: the inner potential correction

Table S3. Comparison of HER performance between the results from the present research with other recently-reported single-atomic electrocatalysts in 1 M KOH.

	HER catalysts	Electrolyte	Overpotentials	Stability	References
1	Ni-N-C/Ni@CNF-H	1 M KOH	177 mV@10 mA cm^{-2}	160 h	In this work
2	Co-N/C	1 M KOH	219 mV@10 mA cm^{-2}	24h	ACS Catal. **2019**, 9, 83-97.
3	Ni NP/Ni-N-C	1 M KOH	147 mV@10 mA cm^{-2}	10 h	Energy Environ. Sci. 2019,12, 149-156
4	Ni@Co/N/C	1 M KOH	181 mV@10 mA cm^{-2}	-	Angew. Chem. Int. Ed. **2019**, 58, 11868.
5	SACo-N/C	1 M KOH	178 mV@10 mA cm^{-2}	35000 s	Sci. Bull. **2019**, 64, 1095.
6	Fe-N_4 SAs/NPC	1 M KOH	202 mV@10 mA cm^{-2}	70000 s	Angew. Chem. Int. Ed. **2018**, 57, 8614.
7	Ni-N-C-250	1 M KOH	400 mV@10 mA cm^{-2}	1000 cycles	Nano Energy **2021**, 83, 105850.
8	Ni-$FePS_3$ NSs/C	1 M KOH	219 mV@10 mA cm^{-2}	-	Energy Environ. Mater. **2022**, 5, 899-905.
9	CoSA + Co_9S_8/HCNT	1 M KOH	250 mV@10 mA cm^{-2}	10 h	Small **2020**, 16, 1906735.

References

[1] Nørskov, J. K.; Rossmeisl, J.; Logadottir, A.; Lindqvist, L.; Kitchin, J. R.; Bligaard, T.; Jónsson, H. Origin of the overpotential for oxygen reduction at a fuel-cell cathode. *J. Phys. Chem. B* **2004**, 108(46), 17886-17892, DOI: 10.1021/jp047349j.

[2] Nørskov, J. K.; Bligaard, T.; Logadottir, A.; Kitchin, J. R.; Chen, J. G.; Pandelov, S.; Stimming, U. Trends in the exchange current for hydrogen evolution. *J. Electrochem. Soc.* **2005**, 152, J23, DOI: 10.1149/1.1856988.

[3] Nørskov, J. K; Abild-Pedersen, F.; Studt, F.; Bligaard, T. Density functional

theory in surface chemistry and catalysis. *Proc. Natl. Acad. Sci. U.S.A.* **2011**, 108(3), 937-943, DOI: 10.1073/pnas.1006652108.

[4] C. Wei, S. N. Sun, D. Mandler, X. Wang, S. Z. Qiao, Z. Xu, Approaches for measuring the surface areas of metal oxide electrocatalysts for determining their intrinsic electrocatalytic activity, *Chem. Soc. Rev.*, 2019, **48**, 2518-2534.

[5] Y. Yang, W. Zhang, Y. Xiao, Z. Shi, X. Cao, Y. Tang, Q. Gao, $CoNiSe_2$ heteronanorods decorated with layered-double-hydroxides for efficient hydrogen evolution, *Appl. Catal. B: Environ.*, 2019, **242**, 132-139.

[6] D. Wu, D. Chen, J. Zhu, S. Mu, Ultralow Ru incorporated amorphous cobalt-based oxides for high-current-density overall water splitting in alkaline and seawater media, *Small*, 2021, **17**, 2102777.

[7] W. Chen, B. Wu, Y. Wang, W. Zhou, Y. Li, T. Liu, C. Xie, L. Xu, S. Du, M. Song, D. Wang, Y. liu, Y. Li, J. Liu, Y. Zou, R. Chen, C. Chen, J. Zheng, Y. Li, J. Chen, S. Wang, Deciphering the alternating synergy between interlayer Pt single-atom and NiFe layered double hydroxide for overall water splitting, Energy Environ. Sci., 2021, 14, 6428-6440.

[8] S. Anantharaj, P. E. Karthik, S. Noda, The significance of properly reporting turnover frequency in electrocatalysis research, Angew. Chem. Int. Ed., 2021, 60, 23051-23067.

[9] S. Liang, T. Zhang, Y. Zheng, T. Xue, Z. Wang, Q. Wang, H. He, Maximizing the utilization of single-atom sites on carbon-based catalysts for efficient CO2 electroreduction with ultrahigh turnover frequency, Appl. Catal. B Environ., 2023, 333, 122801.

[10] T. Luo, J. Huang, Y. Hu, C. Yuan, J. Chen, L. Cao, K. Kajiyoshi, Y. Liu, Y. Zhao, Z. Li, Y. Feng, Fullerene lattice-confined Ru nanoparticles and single atoms synergistically boost electrocatalytic hydrogen evolution reaction, Adv. Funct. Mater., 2023, 33, 2213058.